

pubs.acs.org/ac Article

Measuring Liquid-into-Liquid Diffusion Coefficients by Dissolving Microdroplet Electroanalysis

Ashutosh Rana, Christophe Renault,* and Jeffrey E. Dick*



Cite This: Anal. Chem. 2023, 95, 18748–18753



Read Online

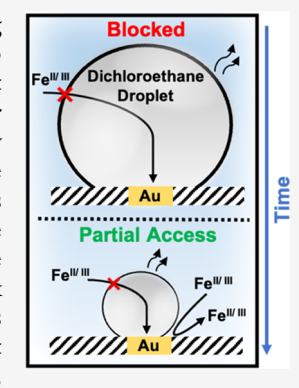
ACCESS I

III Metrics & More

Article Recommendations

SI Supporting Information

ABSTRACT: Diffusion is a fundamental process in various domains, such as pollution control, drug delivery, and isotope separation. Accurately measuring the diffusion coefficients (D) of one liquid into another often encounters challenges stemming from intermolecular interactions, precise observations at the liquid interface, convection, etc. Here, we present an innovative electrochemical methodology for determining the diffusion coefficient of a liquid into another liquid. The method involves precisely tracking the lifetime of a nonaqueous droplet. An organic droplet is placed on an ultramicroelectrode surrounded by an aqueous solution of potassium hexacyanoferrate(II/III). The droplet initially blocks the reduction or oxidation of the redox species. As the droplet dissolves, giving access to the conductive microelectrode surface, a continuously increasing current is observed in voltammetry and the amperometric i-t response. The electrochemical response thus directly reports on the flux of redox species on the electrode surface, allowing us to precisely determine the lifetime of the droplet. D values are directly determined through a combination of electrochemical analysis and the principles of droplet dissolution. We demonstrate the quantification of 1,2-dichloroethane and nitrobenzene into water,



yielding diffusion coefficients of $(11.3 \pm 1.2) \times 10^{-6}$ cm²/s and $(5.2 \pm 1.1) \times 10^{-6}$ cm²/s, respectively. This work establishes a reliable electrochemical approach for quantifying diffusion coefficients based on droplet lifetime analysis.

■ INTRODUCTION

Diffusion refers to the random motion of molecules by which there is a net flow of matter from a region of high concentration to a region of low concentration.^{1,2} The phenomenon of diffusion can be observed in solid, liquid, or gaseous materials.³ It enables process optimization in industrial settings by guiding the design of efficient chemical reactions and separation techniques and modeling the transport and fate of pollutants. The study of diffusion is crucial for applications like liquid—liquid extraction, isotope separation, pollution control, design of chemical reactors, etc.⁴ Moreover, precise values of diffusion coefficients (*D*) are needed for the study of droplet dissolution, fluid mechanics, mass transport, etc.^{5–7}

The value of *D* for a liquid dissolving into another liquid can be obtained either by empirical correlations or experimentally. Unfortunately, empirical correlations fail at higher concentrations and call for experimental methods to accurately determine D values.^{8,9} Various techniques are available for measuring D values for liquid-into-liquid diffusion such as holographic interferometry, Taylor dispersion, nuclear magnetic resonance (NMR), and diaphragm cells. 10-13 Holographic interferometry is based on recording and reconstructing interference patterns to determine the concentration profile and hence the diffusion coefficients of the diffusive solvents. Analyzing interferometry data can be complex and often requires sophisticated mathematical tools and algorithms. Moreover, the experimental condition needs to be precisely controlled as external disturbances, such as vibrations or temperature fluctuations, can introduce noise and affect the

accuracy of measurements.¹⁴ Taylor dispersion is based on the analysis of solute dispersion in a laminar flow. The method uses a refractive index detector to obtain a concentration profile similar to the Gaussian distribution curve. 15 However, the implementation of Taylor dispersion experiments requires precise flow control and sophisticated data analysis methods. Also, the Taylor dispersion method uses a spiral capillary with length up to several meters and the mobile phase is required to flow through the round cross section at a constant flowing rate, which is difficult to achieve and leads to poor accuracy. 16 NMR spectroscopy provides precise measurements of diffusion coefficients. It allows for nondestructive analysis and can provide insights into molecular dynamics. However, NMR techniques require specialized equipment and expertise in data acquisition and analysis and may have limitations related to sample concentration and viscosity. 13 Diaphragm cells consist of two compartments separated by a permeable diaphragm, allowing the solute to diffuse from one compartment to the other. This technique requires monitoring the change in the initial and final concentration in the compartments. However,

Received: July 23, 2023
Revised: November 2, 2023
Accepted: November 2, 2023
Published: December 11, 2023





this technique can be time-consuming and requires precise calibration of the cell. 17,18

The diffusion coefficient of a liquid in another liquid can also be determined by studying the dissolution kinetics of microdroplets and accurately monitoring droplet lifetimes. ^{6,7,19} This is usually done using optical microscopy, dynamic light scattering (DLS), and scanning probe techniques such as atomic force microscopy (AFM). However, these techniques involve tradeoffs between resolution, cost, versatility, and temporal capabilities to accurately quantify the dissolution rate and lifetime of the droplets. ²⁰ For instance, AFM offers nanometer resolution but suffers from poor temporal resolution and optical microscopy suffers from poor spatial resolution close to the diffraction limit of light. ^{21,22}

This study introduces an electrochemical methodology for determining the diffusion coefficients of one liquid in another liquid based on the analysis of droplet lifetimes by physical blocking of the electrode surface. The obtained droplet lifetime data enable the calculation of diffusion coefficients using the dissolution laws. We demonstrate the effectiveness of this approach by accurately tracking the lifetime of 1,2-dichloroethane (DCE) droplet on a gold ultramicroelectrode (UME) immersed in an aqueous phase containing potassium ferricyanide $(K_3[(Fe(CN)_6)])$, potassium ferrocyanide $K_4[(Fe(CN)_6)].3H_2O_1$, and 1 M potassium chloride (KCl) in deionized (DI) water. Blocking of the electrode enables us to accurately determine the lifetime of droplets by using voltammetry and chronoamperometry. Notably, this method of determining the lifetime of the droplet surpasses the other existing techniques in terms of temporal resolution and convenience. Additionally, we extend the application of this methodology to determine the diffusion coefficient of nitrobenzene (NB) in water, highlighting its broad utility for studying different liquid-liquid systems. Overall, this work establishes an innovative and reliable electrochemical approach for quantifying diffusion coefficients based on droplet lifetime analysis.

■ EXPERIMENTAL SECTION

Figure 1 describes the setup used to simultaneously monitor the optical and electrochemical responses of oil microdroplets on a gold UME submerged in the bulk aqueous phase. The aqueous bulk phase consists of a mixture of 10 mM $K_3[(Fe(CN)_6)]$, 5 mM $K_4[(Fe(CN)_6)]$, and 1 M KCl in DI water. A 6.3 µm radius disk gold electrode (see Figure S3a) was held vertically inside a Teflon-made cell filled with the aqueous bulk phase. A microinjection system equipped with a XYZ micropositioner, a compressor, and a microcapillary was used to dispense DCE droplets above the surface of the Au disk. The described setup was equipped with a high-resolution optical camera, which enabled the positioning of the microcapillary as well as tracking the size of the dispensed DCE droplet. All of the electrochemical measurements were performed in a two-electrode setup where the Au UME served as the working electrode and Ag/AgCl in 1 M KCl served as the counter/reference electrode, which was present in a separate reservoir, as shown in Figure 1. The electrical connection was established by using an agarose salt bridge (3% agarose in 1 M KCl). The detailed experimental section can be found in the Supporting Information (SI).

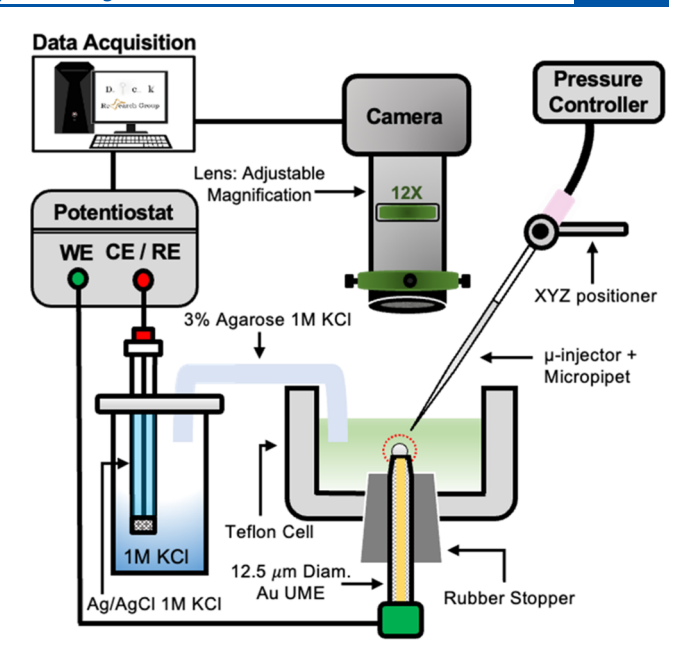


Figure 1. Experimental setup used to visualize droplet dissolution with *in situ* monitoring of the droplet size and simultaneous recording of their electrochemical response. A 6.3 μ m radius Au UME is held vertically in a Teflon cell (gray) containing the aqueous bulk phase (light green). The camera allows precise monitoring of the position of the microcapillary and Au disk. The microinjection system allows us to deliver a small volume of oil droplets on the Au disk. The oil droplet is shown in light gray on the surface of the electrode.

■ RESULTS AND DISCUSSION

A typical experiment consists of microinjecting an oil droplet on the Au disk with time-synchronized electrochemical measurement and in situ monitoring of the droplet size using a high-resolution camera. A series of optical micrographs recorded during a typical experiment is shown in Figure 2a. Time *t* is referenced at 0 s, which marks the time at which we start recording the micrographs. On each micrograph, the bright spot at the center is the Au disk and the red circle marks the perimeter of the electrode, which is surrounded by a glass sheath. Prior to the injection at t = 4 s, the position of the microcapillary used to dispense an oil microdroplet is marked on the right. The initial apparent radius of the droplet is measured to be 45 \pm 3 μ m. The contact angle was measured independently for DCE droplets on glass and was found to be 149° (see Figure S4). It is evident from the micrographs that the droplet maintains its spherical curvature and dissolves into the aqueous phase, centered around the gold UME, within \sim 223 \pm 4 s. During the course of dissolution, the three-phase boundary gets pinned at the Au/glass interface, forcing the droplet to stay centered on the UME. This error originates from the time required for the injection of the DCE droplet and determination of the final time when V_f is zero.

Prior to the injection of the DCE droplet, the electrochemical signals arise solely due to the electron transfer associated with $Fe(CN)_6^{4-}$ and $Fe(CN)_6^{3-}$ present in the aqueous bulk phase. The cyclic voltammogram for the bulk aqueous phase in the absence of a droplet is shown in Figure S3b. $K_3[(Fe(CN)_6)]$ and $K_4[(Fe(CN)_6)]$ were chosen for these experiments because they are particularly insoluble in oil and will remain in the aqueous phase in the presence of an oil droplet allowing the oil droplet to block the electrochemical response of the $Fe(CN)_6^{4-}$ and $Fe(CN)_6^{3-}$ present in the

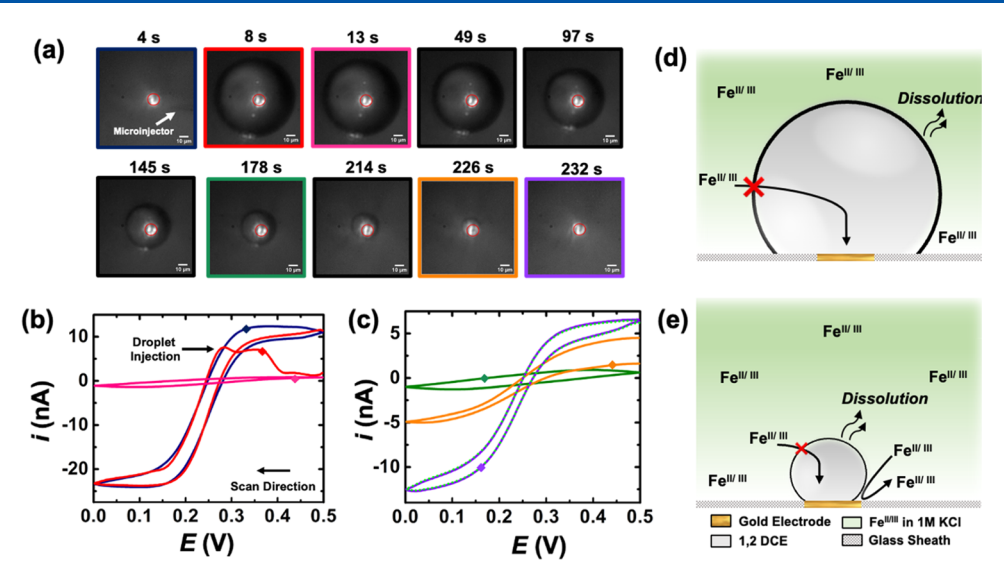


Figure 2. (a) Optical micrographs recorded during the dissolution of a $45 \pm 3 \mu m$ radius DCE droplet in the aqueous bulk phase. The solid red line on the micrograms indicated the position of the Au disk. The scale bar is $10 \mu m$. (b) and (c) Cyclic voltammograms recorded at a scan rate of 0.2 V/s, simultaneously with the optical micrographs during the dissolution of the DCE droplet. The voltammograms are color-coded and match the color code in (a), and the colored points on the voltammogram denote the time at which the micrographs in (a) were recorded. The raw data for the voltammograms had to be smoothed to filter out the noise (because a Faraday cage was not used) using adjacent weighted averaging and a Savitzky–Golay filter. (d) and (e) Mechanism of blocking of flux of redox analyte as a function of droplet size.

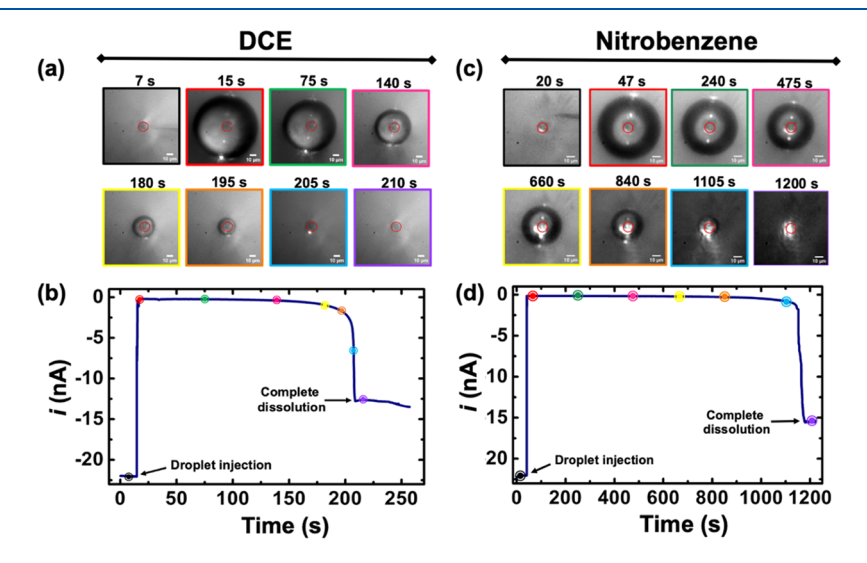


Figure 3. (a) Optical micrographs recorded during the dissolution of a $49 \pm 3 \mu m$ radius DCE droplet in the aqueous bulk phase. The solid red line in the micrographs indicate the position of the Au disk. The scale bar is $10 \mu m$. (b) i-t response to an applied potential of 0 V, simultaneously with the optical micrographs during the dissolution of the DCE droplet. The i-t response is color-coded and matches the color code in (a), and the colored points on the i-t response denote the time at which the micrographs in (a) were recorded. (c) Similar to (a) showing the dissolution of a $36 \pm 3 \mu m$ radius nitrobenzene droplet. (d) Generated i-t response. The contact angle was measured independently for NB droplets on glass and was found to be 155° (see Figure S5). Again, the colored points of the i-t response in (d) denote the exact time at which micrographs in (d) were recorded for a nitrobenzene droplet.

aqueous bulk phase until the final moments of dissolution of the droplet. This phenomenon was examined using cyclic voltammetry and chronoamperometry and is discussed in detail in the following paragraphs.

Along with monitoring the geometry of the droplet, the electrochemical response was recorded as a function of time. The potential of the UME is constantly scanned at a rate of 0.2 V/s, between 0 and 0.5 V (5 s per voltammogram). The potential window is centered around the apparent standard potential of the redox couple $Fe(CN)_6^{3-}/Fe(CN)_6^{4-}$, $E^{\circ\prime}=0.2$ V, which is evident from the voltammetry of the bulk phase shown in Figure S3b. The optical micrographs and voltammo-

grams are color-coded such that colored points and segments (Figure 2b,c) correspond to the time at which micrographs (Figure 2a) were recorded. In the absence of any droplet at t=4 s, a sigmoidal voltammogram is obtained, which is typical of voltammetry at a UME in a bulk phase containing redox active species. The anodic and cathodic current plateaus prior to the injection of the droplet are observed at 10 and -23 nA, respectively (denoted by the dark blue curve in Figure 3b). The injection appears as a sudden decrease in current (red curve in Figure 2b) to a few nanoamperes due to the physical blocking of the electrode by the DCE droplet, following which no redox activity is observed around the apparent standard

potential of the $Fe(CN)_6^{3-}/Fe(CN)_6^{4-}$ redox couple (pink curve in Figure 2b). As the droplet continues to dissolve, no redox activity is observed until an apparent radius of the droplet is $\sim 15 \ \mu m$ (orange frame in Figure 2a), which corresponds to a contact radius of $\sim 8 \mu m$, after which the magnitude of current gradually increases (orange and purple curves in Figure 2c) as the droplet further shinks. The mechanism of electrode blocking due to the presence of the droplet is illustrated in Figure 2d,e, which shows when the droplet size is large, hence it's contact area is large compared to the Au disk, the redox species in the bulk phase has no access to the electrode. When the contact area is comparable to the size of the Au disk, the redox species in the bulk gain partial access to the electrode, giving rise to an increase in the magnitude of current, as shown in Figure 2c. Therefore, as the droplet shrinks beyond a critical size, the electrode gains access to the redox species present in the bulk phase due to partial exposure of the Au disk. For example, notice the micrographs recorded at 226 s (orange frame) in Figure 2a: the droplet is physically present, but the magnitude to current on the corresponding voltammogram is not the same as when the droplet is large, submerging the entire Au disk. This critical size is achieved when the contact lines approach the Au disk and the mode of dissolution switches from the constant contact angle mode to the constant contact radius mode. The details of the dissolution kinetics of sessile droplets and droplets dissolving on the surface of a Au disk UME are shown in the SI. Notice that after the complete dissolution of the droplet, the anodic and cathodic current plateaus do not converge to the same values noted prior to the droplet injection. The dashed cyan curve overlaid on the violet curve in Figure 2c is the voltammogram recorded minutes after the complete evaporation of the droplet, and the anodic and cathodic steady-state current still does not converge to the initial values. This strongly indicates the presence of waterphase inclusions in the DCE droplet, which (salt) precipitates over time, leading to partial coverage of the electrode surface with salt precipitate and hence the reduced magnitude of anodic and cathodic current plateaus. 23,24 The exact reason for the discrepancy in initial and final steady-state currents is unknown and represents a future avenue of our work.

The voltammetry experiments provide valuable insights into the process of physical blocking of the electrode by a DCE droplet. However, to determine the diffusion coefficient of DCE in water, the lifetime of the droplet needs to be precisely determined, which is not possible using voltammetry due to the poor temporal resolution that is dictated by the scan rate. To accurately determine the lifetime of the oil droplets, chronoamperometry was performed at the mass transport conditions observed from Figure 2b,c, which are the potentials at which steady-state currents are observed (i.e., 0 V vs Ag/ AgCl in 1 M KCl for reduction of $Fe(CN)_6^{3-}$ to $Fe(CN)_6^{6-}$ and 0.5 V vs Ag/AgCl in 1 M KCl for oxidation of Fe(CN)₆⁴⁻ to $Fe(CN)_6^{3-2}$ Figure 3a is similar to Figure 2a, which shows the dissolution of a DCE droplet on the Au disk, but here, the potential of the electrode is held at at a constant value of 0 V vs Ag/AgCl during the entire dissolution process. Again, time t is referenced at 0 s, which marks the time at which we start recording the micrographs. Droplet injection occurs at 15 s, with an apparent droplet radius of 49 \pm 3 μ m (red frame in Figure 3a). As shown in Figure 3b, the initial current is -23nA, which is equal to the cathodic current plateau observed from the dark blue curve in Figure 2b. After the injection of the

droplet, the current abruptly decreases to a few nanoamperes due to the blocking of the electrode surface by the DCE. After the droplet shrinks to an apparent radius of $16 \pm 3 \mu m$ (yellow frame in Figure 3a), the current steadily increases (see Figure 3b). This increase in current after 150 s in Figure 3b can be attributed to partial exposure of the Au disk, which allows the reduction of $Fe(CN)_6^{3-}$ to $Fe(CN)_6^{4-}$ at these exposed sites (similar to voltammetry results). The extent of the exposure increases as the droplet further shrinks with time. After the complete evaporation of the droplet, the current magnitude returns to a new value of steady-state current of ~13 vs 23 nA before droplet injection (similar to the reduced value of cathodic current plateau observed after complete dissolution of the droplet in cyclic voltammetry). While the exact nature of this new steady-state current is not yet fully understood, the experiment still allows us to quantify droplet lifetimes with high precision. It is essential to note that in the i-t response, there is a characteristic change that marks the complete dissolution of the droplet that was absent in cyclic voltammetry. Movie S1 shows the side-by-side evolution of the *i*–*t* response and droplet size for the data shown in Figure 3a,b. Moreover, chronoamperometry allows us to record data at a much higher temporal resolution than voltammetry, enabling us to precisely determine the lifetime of the DCE droplets in the aqueous bulk phase. We now define $\tau_{\rm echem}$ as the lifetime of the DCE droplet (time duration between the initial abrupt decrease in current to the time taken for attainment of a new steady-state current) using chronoamperometry, which equals 195 s based on Figure 3b. Note that this method to determine the droplet lifetime using the i-tresponses could be done for either oxidation or reduction of redox species in the bulk. We also note that the accuracy by which we can measure au_{echem} is based only on the temporal resolution of our measurement and the signal-to-noise ratio and not a fundamental limitation, such as the diffraction limit of light. Figure 3b shows the i-t response for the reduction of $Fe(CN)_6^{3-}$ to $Fe(CN)_6^{4-}$, but a similar response would be observed for the oxidation of $Fe(CN)_6^{4-}$ to $Fe(CN)_6^{3-}$ too. Figure S6a shows the i-t response where electrode potential was held at 0.5 V vs Ag/AgCl for a DCE droplet with an initial apparent radius of $57 \pm 3 \mu m$ (Figure S6b). This also explains the choice of the composition of analytes in the aqueous continuous phase, where both Fe(CN)₆⁴⁻ and Fe(CN)₆³⁻ species were present, to demonstrate that the methodology for determining the droplet lifetime is independent of the redox probe present.

From the data given in Figure 3, we can determine the value of $D_{\rm DCE \rightarrow water}$. The methodology for determining $D_{\rm DCE \rightarrow water}$ based on the initial droplet size and $\tau_{\rm echem}$ using eqs S7–S11 is detailed in the SI.

Table 1 shows the calculated $D_{\rm DCE \to water}$ values based on the initial droplet radius and $\tau_{\rm echem}$. It is evident from Table 1 that $\tau_{\rm echem}$ is longer for droplets with a larger initial radius. This is because of a strong dependence of eqs S3 and S4 on the initial radius of the droplet. Based on the results stated in Table 1, $D_{\rm DCE \to water}$ was found to be $(11.3 \pm 1.2) \times 10^{-6}$ cm²/s. This value of $D_{\rm DCE \to water}$ is in close agreement with the values reported in the literature. The same methodology was used to determine the diffusion coefficient of nitrobenzene (NB) in an aqueous bulk phase. Figure 3c,d shows the dissolution of a $36 \pm 3~\mu \rm m$ NB droplet in the same bulk phase as before with the simultaneous recording of the i-t response at a potential of 0 V vs Ag/AgCl in 1 M KCl. The behavior is again similar to

Table 1. Calculated Diffusion Coefficient for DCE in Water as a Function of the Initial Radius of the Droplet (R_i) and Lifetime of the Droplet $(\tau_{\rm echem})$ Determined Using Chronoamperometry

$R_i (\mu m)$	$ au_{ m echem}$ (s)	$D(cm^2/s)$
43	201	9.9×10^{-6}
44	190	11.1×10^{-6}
49	195	13.3×10^{-6}
54	258	12×10^{-6}
57	334	10.4×10^{-6}

the case of the DCE droplet with an initial steady-state current of ~23 nA with an abrupt decrease in current to a few nanoamperes after the injection of the droplet, followed by a steady increase in current when the droplet's apparent radius is $13 \pm 3 \mu m$ (blue frame in Figure 3c), followed by complete dissolution and a new steady-state current (-16 nA). The lifetime of the NB droplet based on Figure 3d for an initial radius of 36 \pm 3 μ m was found to be 1135 s. Table S1 shows the $D_{\mathrm{NB} o \mathrm{water}}$ values based on the initial droplet radius and $au_{\rm echem}$ for NB in water, which yields a value of (5.2 \pm 1.1) \times 10⁻⁶ cm²/s (see Table S1). This value is lower than the values (typically $8.6 \times 10^{-6} \text{ cm}^2/\text{s}$ to $10.4 \times 10^{-6} \text{ cm}^2/\text{s}$ at 26 °C) reported in the literature. 26-29 We anticipated the diffusion coefficient of NB to be lower than that of DCE molecules due to the larger size of NB than that of DCE. The discrepancy in the diffusion coefficient for NB compared to literature values can perhaps be explained by differences in measurement techniques. Previous measurements have employed techniques like Taylor dispersion; however, our electrochemical technique, measured at the steady state, is perhaps more representative of the true diffusion coefficient.

Despite very comparable initial sizes of DCE and NB droplets, 49 and 36 μ m, respectively, the time taken for complete dissolution of the DCE and NB droplets is significantly different (195 s for DCE and 1135 s for NB), but the value of the diffusion coefficient is comparable for both of them. This arises due to striking differences in the saturation concentration, i.e., 0.0023 g/cm³ for NB and 0.0087 g/cm³ for DCE. Therefore, the methodology detailed in the work can be used for any other oil droplet dissolving in the bulk aqueous phase.

CONCLUSIONS

In conclusion, this study introduces an electrochemical methodology utilizing chronoamperometry to determine the diffusion coefficients of a liquid in liquid. The work is based on a comprehensive analysis of the lifetime of oil droplets using chronoamperometry, where the current starts off at a steady state, experiences an abrupt decrease due to the physical blocking of the electrode caused by the oil droplet, and subsequently increases steadily as the droplet shrinks over time. The complete dissolution of the droplet is marked by the attainment of a new steady-state current. The determined lifetime, in conjunction with equations describing droplet dissolution on a UME submerged in an aqueous bulk phase, enables the calculation of the diffusion coefficient of oil in water. This work not only presents a valuable approach for determining diffusion coefficients but also offers a reliable means of assessing droplet lifetimes in various applications.

ASSOCIATED CONTENT

Solution Supporting Information

The Supporting Information is available free of charge at https://pubs.acs.org/doi/10.1021/acs.analchem.3c03256.

Evolution of the i-t response and droplet size (MP4)

Experimental section; dissolution kinetics and lifetimes of sessile droplets; geometrical description of the droplet; cyclic voltammograms of 10 mM K_3 [(Fe-(CN)₆)], 5 mM K_4 [Fe(CN)₆]·3H₂O, and 1 M KCl in DI water using a 6.35 μ m radius Au UME; contact angle measurements for DCE and NB droplets in water; i-t response to an applied potential of 0.5 V vs Ag/AgCl for oxidation of Fe(CN)₆⁴⁻ to Fe(CN)₆³⁻; theoretical framework for determining the lifetime of droplets using dissolution laws; and table for the diffusion coefficient of NB in water (PDF)

AUTHOR INFORMATION

Corresponding Authors

Christophe Renault — Department of Chemistry, Purdue University, West Lafayette, Indiana 47907, United States; orcid.org/0000-0003-4525-8702; Email: crenault@purdue.edu

Jeffrey E. Dick — Department of Chemistry, Purdue University, West Lafayette, Indiana 47907, United States; Elmore Family School of Electrical and Computer Engineering, Purdue University, West Lafayette, Indiana 47907, United States; orcid.org/0000-0002-4538-9705; Email: jdick@purdue.edu

Author

Ashutosh Rana – Department of Chemistry, Purdue University, West Lafayette, Indiana 47907, United States

Complete contact information is available at: https://pubs.acs.org/10.1021/acs.analchem.3c03256

Notes

The authors declare no competing financial interest.

ACKNOWLEDGMENTS

This work was funded by the Chemical Measurement and Imaging Program of the National Science Foundation under grant CHE-2003587/2319925.

■ REFERENCES

- (1) Harteck. Angew. Chem. 1953, 65 (19), 496.
- (2) Bard, A. J.; Faulkner, L. R. Electrochemical Methods: Fundamentals and Applications; John Wiley & Sons: New York, 2001.
- (3) Bird, R. B.; Stewart, W. E.; Lightfoot, E. N. Transport Phenomena; John Wiley & Sons: New York, 2002.
- (4) Cussler, E. L. Diffusion: Mass Transfer in Fluid Systems, 3rd ed.; Cambridge University, 2009; p 2009.
- (5) He, M. G.; Zhang, S.; Zhang, Y.; Peng, S. G. Opt Express 2015, 23 (9), 10884.
- (6) Stauber, J. M.; Wilson, S. K.; Duffy, B. R.; Sefiane, K. J. Fluid Mech. 2014, 744, 744.
- (7) Popov, Y. O. Phys. Rev. E: Stat., Nonlinear, Soft Matter Phys. **2005**, 71 (3), No. 036313, DOI: 10.1103/PhysRevE.71.036313.
- (8) Dhiraj, P. Measurement of Diffusivity Using Laser Optical Interferometry, ME (Chem. Engg.) Dissertation, MS University of Baroda, 2000.

- (9) Chhaniwal, V. K.; Anand, A.; Girhe, S.; Patil, D.; Subrahmanyam, N.; Narayanamurthy, C. S. J. Opt. A: Pure Appl. Opt. 2003, 5, No. S329.
- (10) Riquelme, R.; Lira, I.; Pérez-López, C.; Rayas, J. A.; Rodríguez-Vera, R. *J. Phys. D: Appl. Phys.* **2007**, 40 (9), 2769–2776.
- (11) Stokes, R. H. J. Am. Chem. Soc. 1950, 72 (2), 763-767.
- (12) Leaist, D. G.; Hao, L. J. Phys. Chem. A 1994, 98 (17), 4702–4706.
- (13) Evans, R.; Poggetto, G. D.; Nilsson, M.; Morris, G. A. Anal. Chem. 2018, 90 (6), 3987–3994.
- (14) Guo, Z.; Maruyama, S.; Komiya, A. J. Phys. D: Appl. Phys. 1999, 32. 995.
- (15) Cipelletti, L.; Biron, J. P.; Martin, M.; Cottet, H. Anal. Chem. **2015**, 87 (16), 8489–8496.
- (16) Van De Ven-Lucassen, I. M. J. J.; Kieviet, F. G.; Kerkhof, P. J. A. M. J. Chem. Eng. Data 1995, 40 (2), 407-411.
- (17) Zhao, C.; Li, J.; Ma, P. Opt. Laser Technol. 2006, 38 (8), 658-662.
- (18) Toor, H. L. J. Phys. Chem. A 1960, 64 (10), 1580-1582.
- (19) Dietrich, E.; Kooij, E. S.; Zhang, X.; Zandvliet, H. J. W.; Lohse, D. *Langmuir* **2015**, *31* (16), 4696–4703.
- (20) Rana, A.; Renault, C.; Dick, J. E. Understanding Dynamic Voltammetry in a Dissolving Microdroplet (Unpublished).
- (21) Kurra, N.; Scott, A.; Kulkarni, G. U. Nano Res. 2010, 3 (5), 307-316.
- (22) Gonçalves, M.; Kim, J. Y.; Kim, Y.; Rubab, N.; Jung, N.; Asai, T.; Hong, S.; Weon, B. M. Sci. Rep. **2022**, 12 (1), No. 1087, DOI: 10.1038/s41598-022-04877-w.
- (23) Glasscott, M. W.; Voci, S.; Kauffmann, P. J.; Chapoval, A. I.; Dick, J. E. *Langmuir* **2021**, *37* (9), 2907–2912.
- (24) Voci, S.; Clarke, T. B.; Dick, J. E. Chem. Sci. 2023, 14 (9), 2336-2341.
- (25) Intermedia Transfer Factors for Contaminants Found at Hazardous Waste Sites 1,2 DICHLOROETHANE (DCA); Department of Environmental Toxicology University of California Davis, CA, 1994.
- (26) Chemical Properties for Calculation of Impact to Ground Water Soil Remediation Standards; New Jersey Department of Environmental Protection, 2008.
- (27) Smallwood, I. M. Handbook of Organic Solvent Properties; John Wiley & Sons: New York, 1996.
- (28) PubChem Compound Summary for CID 7416, Nitrobenzene, 2004. https://pubchem.ncbi.nlm.nih.gov/compound/Nitrobenzene (accessed Nov 1, 2023).
- (29) Han, P.; Bartels, D. M. J. Phys. Chem. A 1996, 100 (13), 5597-5602.

☐ Recommended by ACS

Levitating Droplet Electroanalysis

Lynn E. Krushinski, Jeffrey E. Dick, et al.

FEBRUARY 05, 2024

ANALYTICAL CHEMISTRY

READ **C**

Nonsteady-State Electric Circuit in Electrophoresis on Paper: Thermal Consideration of Electrophoretic Lateral-Flow Assays

Nikita A. Ivanov, Sergey N. Krylov, et al.

FEBRUARY 07, 2024

ANALYTICAL CHEMISTRY

READ 🗹

Imaging Single H₂ Nanobubbles Using Off-Axis Dark-Field Microscopy

Milomir Suvira, Bo Zhang, et al.

OCTOBER 18, 2023

ANALYTICAL CHEMISTRY

READ

Determination Method of Diffusion Coefficient in a Neat Redox-Active Ionic Liquid at a Microdisk Electrode in the Domains Ranging from the Steady-State to Potentiodynam...

Hironobu Tahara, Takamasa Sagara, et al.

JUNE 19, 2023

ANALYTICAL CHEMISTRY

READ 🗹

Get More Suggestions >